Electronic Supplementary Material (ESI) for Environmental Science: Water Research & Technology.
This journal is © The Royal Society of Chemistry 2024

Cation-π-induced mixed-matrix nanocomposite for detection and removal of Hg^{2+} and azinphos-methyl towards environment remediation

Kamalpreet Kaur[†], Gagandeep Singh[‡], Navneet Kaur[§,*], Narinder Singh[†,*]

[†]Department of Chemistry, Indian Institute of Technology Ropar, Rupnagar, Punjab 140001, India

[‡]Department of Biomedical Engineering, Indian Institute of Technology Ropar, Rupnagar, Punjab 140001, India

[§]Department of Chemistry, Panjab University, Chandigarh 160014, India

Corresponding author's E-mail: nsingh@iitrpr.ac.in; navneetkaur@pu.ac.in

S.No.	Title
Figure S1	Synthesis of Ionic liquid (IL)
Figure S2	HRMS spectrum of KP-1
Figure S3	HRMS of precursor A
Figure S4	HRMS spectrum for precursor A
Figure S5	^{13}C NMR spectra of precursor A
Figure S6	HRMS spectrum of KP-2
Figure S7	^{1}H NMR spectra of KP-2
Figure S8	^{13}C NMR spectra of KP-2
Figure S9	HRMS of IL
Figure S10	^{1}H NMR spectrum of IL
Figure S11	Composite fabricated membranes
Figure S12	EDAX spectrum of bare **MWCNT**
Figure S13	EDAX spectrum of **IL@MWCNTs**
Figure S14	TGA-DSC analysis of **MWCNTs**
Figure S15	XPS spectrum of full region
Figure S16	Peak table showing the atomic % of elements present in the **Hg/IL@MWCNTs** composite
Figure S17	Relative intensity ratios of D/G, G'/G, and G'/D peaks of pristine **MWCNTs**, **IL@MWCNTs** and **Hg/IL@MWCNTs**.
Figure S18	FTIR spectra of **IL** and **IL@MWCNTs+Hg^{2+}**
Figure S19	(A), (B), (C), (D) and (E) Bright field FE-SEM images of **Hg/IL@MWCNTs**, Elemental mapping of **Hg/IL@MWCNTs** and (F) EDAX of **Hg/IL@MWCNTs**
Figure S20	(A) Comparative cyclic voltammetry graphs of **bare GCE, MWCNTs@GCE, IL/GCE**, **IL@MWCNTs/GCE** and **Hg/IL@MWCNTs/GCE**, (B) EIS plot and cyclic voltammetry profiles of **bare GCE**, **IL@MWCNTs/GCE** and **Hg/IL@MWCNTs/GCE** at frequency 50 to 3×10^{6} Hz, (C) Cyclic voltammetry graphs of **bare GCE**, **IL@MWCNTs/GCE** and **Hg/IL@MWCNTs/GCE** in mixture of 0.1 M KCl consisting $K_3[Fe(CN)_6]$ and $K_4[Fe(CN)_6]$, (D) Comparative profiles of active surface area with differently modified electrodes, (E) Cyclic voltammetry response of **Hg/IL@MWCNTs/GCE** with varying scan rates from 20 to 220 mV/s in a mixture 0.1 M KCl consisting of $K_3[Fe(CN)_6]$ and $K_4[Fe(CN)_6]$ solution and (F) Linear regression plot showing relationship between cathodic and anodic peak currents vs square root of scan rate.
Figure S21	(A) Adsorption capacities of IL@MWCNTs with regard to Hg^{2+} adsorption and (B) Frendulich adsorption isotherm plots for Hg^{2+} adsorption onto IL@MWCNTs**.**

Figure S22	Leaching study of IL@MWCNTs for Hg^{2+} ion
Figure S23	Effect of pH on cathodic current after addition of AZM
Figure S24	DPV response of **Hg/IL@MWCNTs** (A) nitroaromatics; (B) polysaccharides; (C) Vitamins and (D) Bar graph showing the stability of response of **Hg/IL@MWCNTs** for AZM detection with number of days.
Figure S25	Mass spectra of degraded AZM products
Figure S26	^{31}P NMR spectrum obtained for AZM in presence of **Hg/IL@MWCNTs** catalyst in DMSO-d_6:D_2O (35:65 v/v).
Table S1	AZM determination in water
Figure S27	Contact angle measurement
Table S2	Surface area and pore volume of differently modified membranes
Figure S28.	Influence of pH on adsorption kinectics of Hg^{2+} ion
Table S3	Degradation efficiency of membrane towards AZM
Figure S29.	Fe-SEM image of (A) pristine membrane, (B) PA/IL@MWCNTs membrane and (C) after filteration of Hg^{2+} and AZM.
Figure S30.	Influence of pH on AZM adsorption
Table S4	Comparison with literature reports

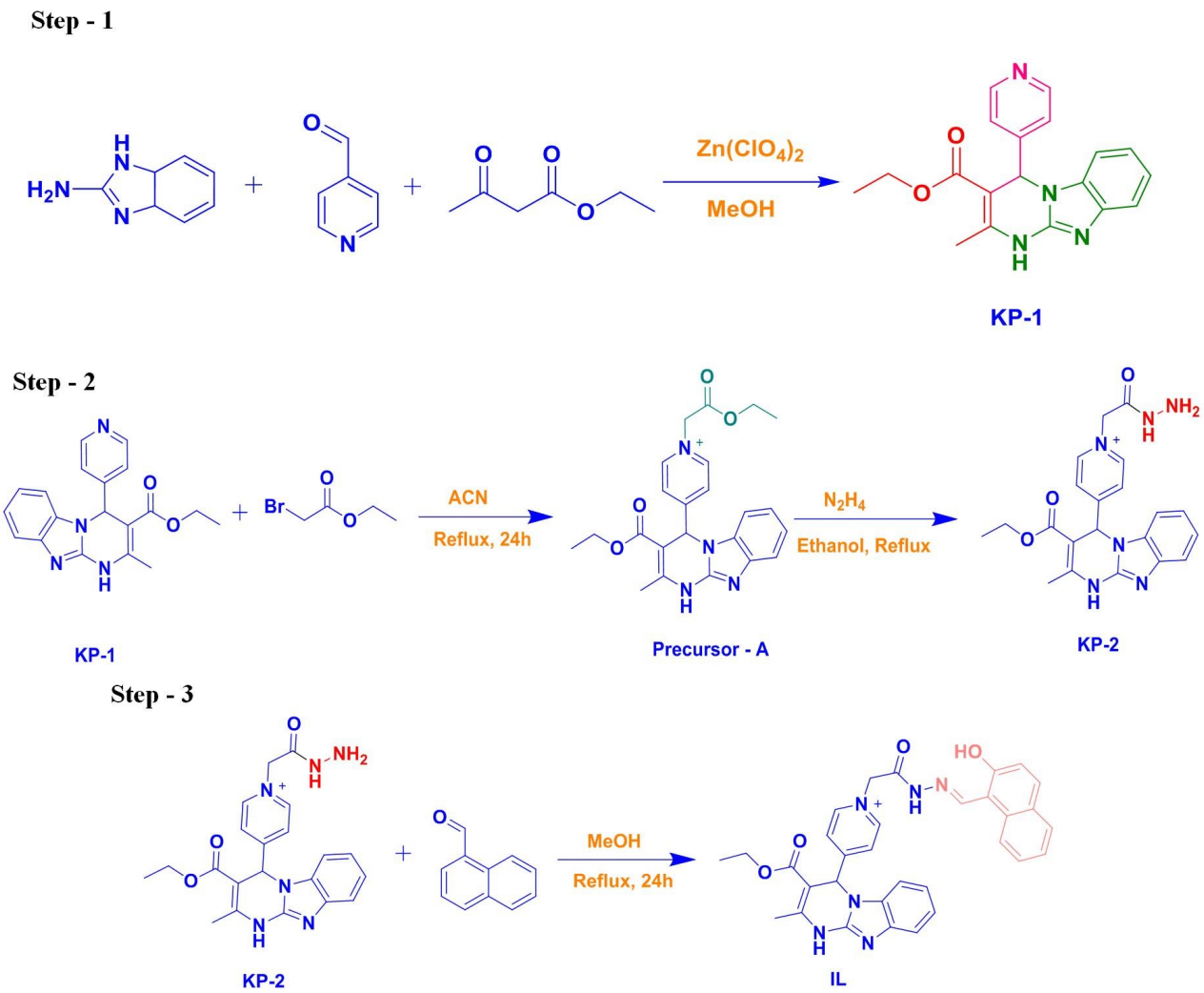

Figure S1. Synthesis of organic cation (IL).

Elemental Composition Report **Page 1**

Single Mass Analysis
Tolerance = 5.0 mDa / DBE: min = -1.5, max = 50.0
Element prediction: Off
Number of isotope peaks used for i-FIT = 3

Monoisotopic Mass, Even Electron Ions
54 formula(e) evaluated with 1 results within limits (up to 50 closest results for each mass)
Elements Used:
C: 19-19 H: 1-100 N: 1-7 O: 1-8

290823_KK-335 17 (0.197) Cm (17:24)

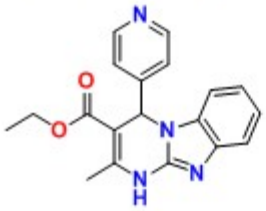

1: TOF MS ES+
4.93e+007

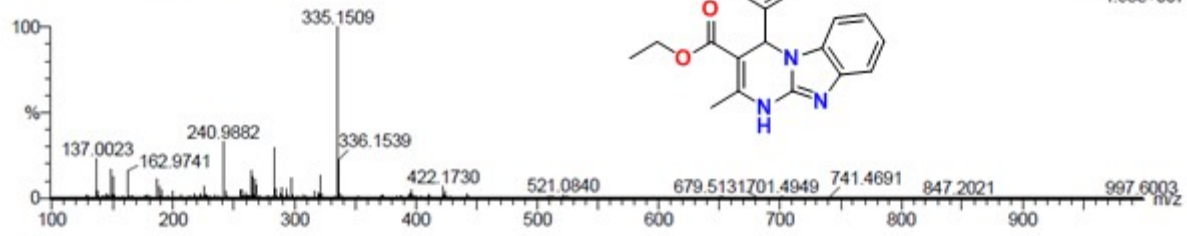

Minimum:				-1.5				
Maximum:		5.0	20.0	50.0				
Mass	Calc. Mass	mDa	PPM	DBE	i-FIT	Norm	Conf(%)	Formula
335.1509	335.1508	0.1	0.3	12.5	1077.4	n/a	n/a	C19 H19 N4 O2

Figure S2. HRMS spectrum of KP-1
HRMS (ESI,m/z): calculated for $C_{19}H_{18}N_4O_2$ [M+1], 335.1508, found 335.1509

Elemental Composition Report **Page 1**

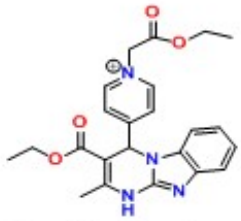

Single Mass Analysis
Tolerance = 5.0 mDa / DBE: min = -1.5, max = 50.0
Element prediction: Off
Number of isotope peaks used for i-FIT = 3

Monoisotopic Mass, Even Electron Ions
20 formula(e) evaluated with 1 results within limits (up to 50 best isotopic matches for each mass)
Elements Used:
C: 0-23 H: 0-25 N: 0-4 O: 0-4

Sample Name : 13:31:19KK-74 IITRPR XEVO G2-XS QTOF
Test Name :
181022-KK-74 17 (0.197)

1: TOF MS ES+
7.93e+006

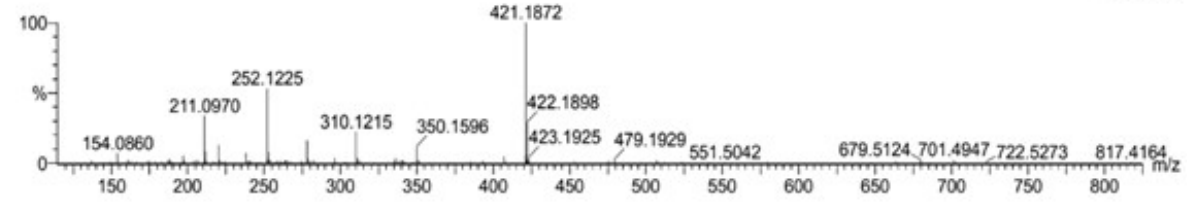

Minimum:				-1.5				
Maximum:		5.0	10.0	50.0				
Mass	Calc. Mass	mDa	PPM	DBE	i-FIT	Norm	Conf(%)	Formula
421.1872	421.1876	-0.4	-0.9	13.5	879.7	n/a	n/a	C23 H25 N4 O4

Figure S3. HRMS of precursor A
HRMS (ESI,m/z): calculated for $C_{23}H_{25}N_4O_4$ $[M]^+$, 421.1876, found 421.1872

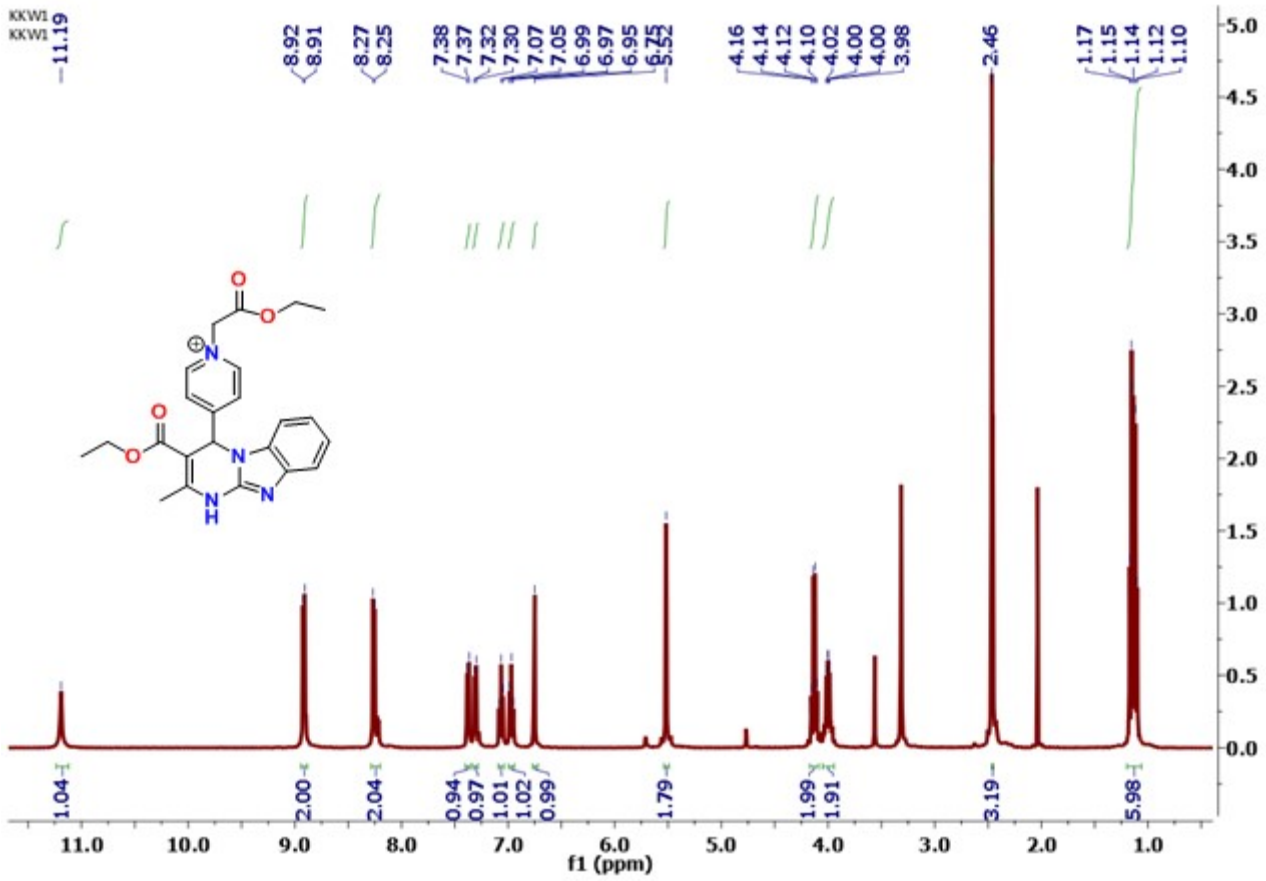

Figure S4. HRMS spectrum for precursor A

^{1}H NMR (400 MHz, DMSO-d6)- δ 11.19 (s, NH, 1H), 8.92 (d, Ar-H, 2H), 8.26 (d, Ar-H, 2H), 7.38 (d, Ar-H, 1H), 7.31 (d, Ar-H, 1H), 7.07 (t, Ar-H, 1H), 6.97 (t, Ar-H, 1H), 6.75 (s, 1H), 5.52 (s, 2H), 4.13 (q, 2H), 4.00 (m, 2H), 2.46 (s, 3H), 1.14 (m, 6H).

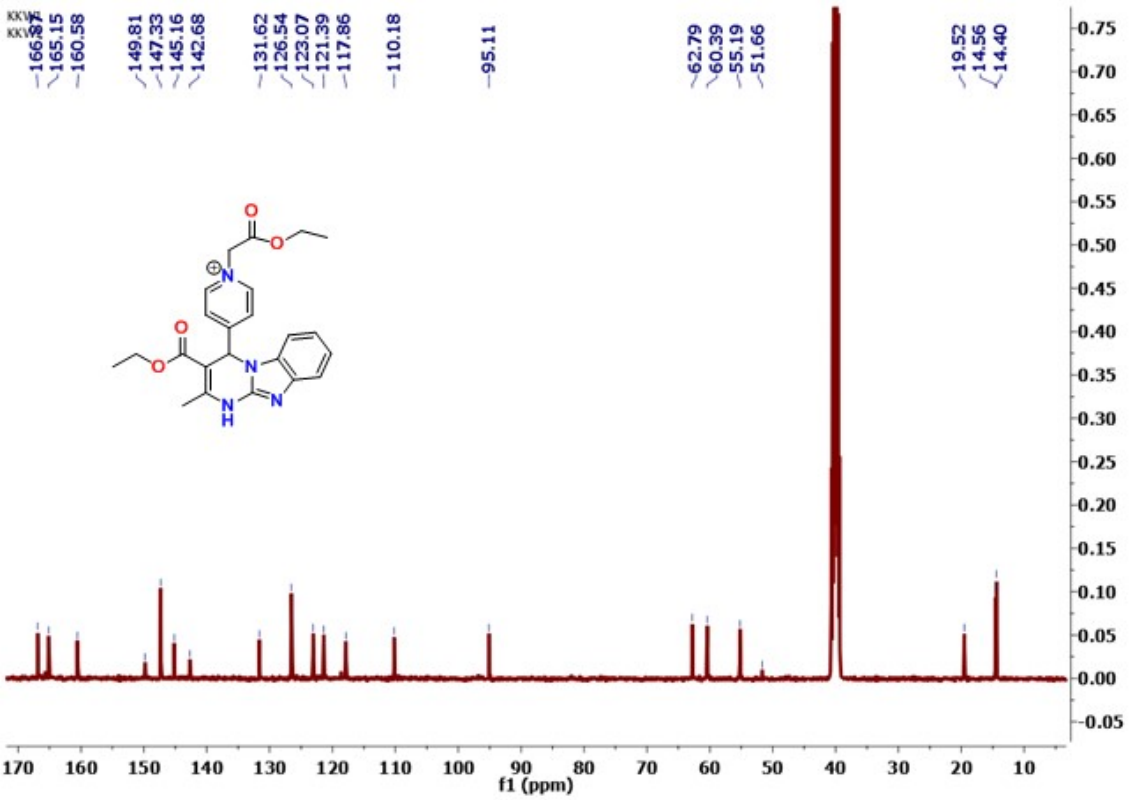

Figure S5. ^{13}C NMR spectra of precursor A

^{13}C NMR (100 MHz in DMSO-d6) - δ 166.8, 165.1, 160.5, 149.8, 147.3, 145.1, 142.6, 131.6, 126.5, 123.0, 121.3, 117.8, 110.1, 95.1, 62.7, 60.3, 55.1, 51.6, 19.5, 14.5, 14.4.

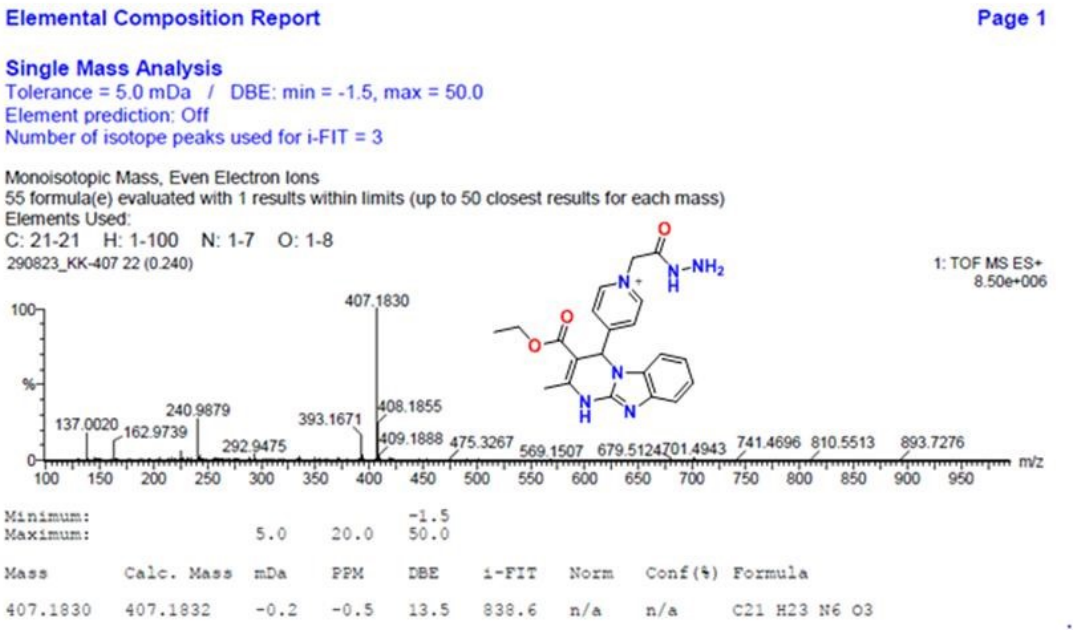

Figure S6. HRMS spectrum of KP-2

HRMS (ESI,m/z): calculated for $C_{21}H_{26}N_6O_3$ $[M]^+$, 407.1832, found 421.1830

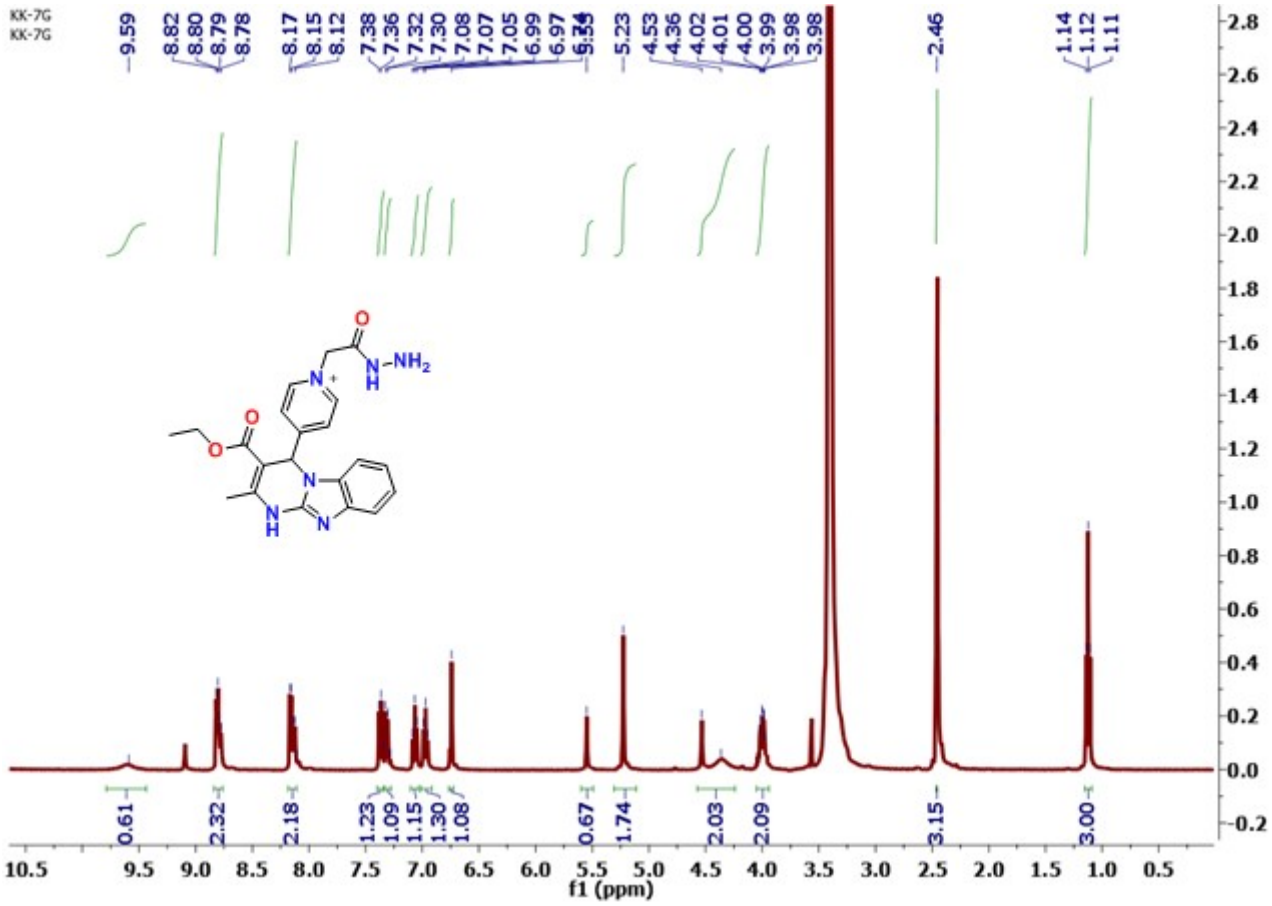

Figure S7. ^{1}H NMR spectra of KP-2

^{1}H NMR (400 MHz in DMSO-d_6)- δ 9.59 (s, -NH, 1H), 8.82-8.78 (m, Ar-H, 2H), 8.17-8.10 (m, Ar-H, 2H), 7.38-7.35 (t, J= 7.36, Ar-H, 1H), 7.32-7.28 (m, Ar-H, 1H), 7.08-7.05 (t, J= 7.07, Ar-H, 1H), 6.99-6.95 (t, Ar-H, 1H), 6.74 (s, -CH, 1H), 5.55 (s, -NH, 1H), 5.23 (s, CH_2, 2H), 4.53 (d, -NH, 2H), 4.01-3.98 (q, -CH_2, 2H), 2.46 (s, CH_3, 3H), 1.14-1.11 (t, J=1.12, CH_3, 3H).

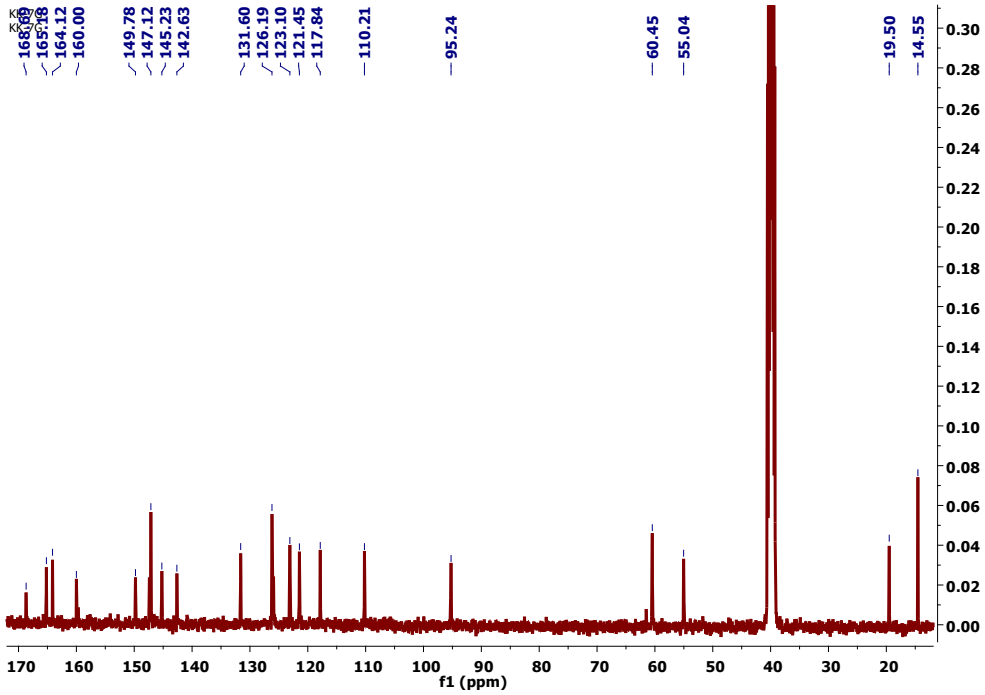

Figure S8. ^{13}C NMR spectra of KP-2

^{13}C NMR (100 MHz in DMSO-d$_6$)- δ 168.6, 165.1, 164.1, 160.0, 149.7, 147.1, 145.2, 142.6, 131.6, 126.1, 123.1, 121.4, 117.8, 110.2, 95.2, 60.4, 55.0, 19.5, 14.5

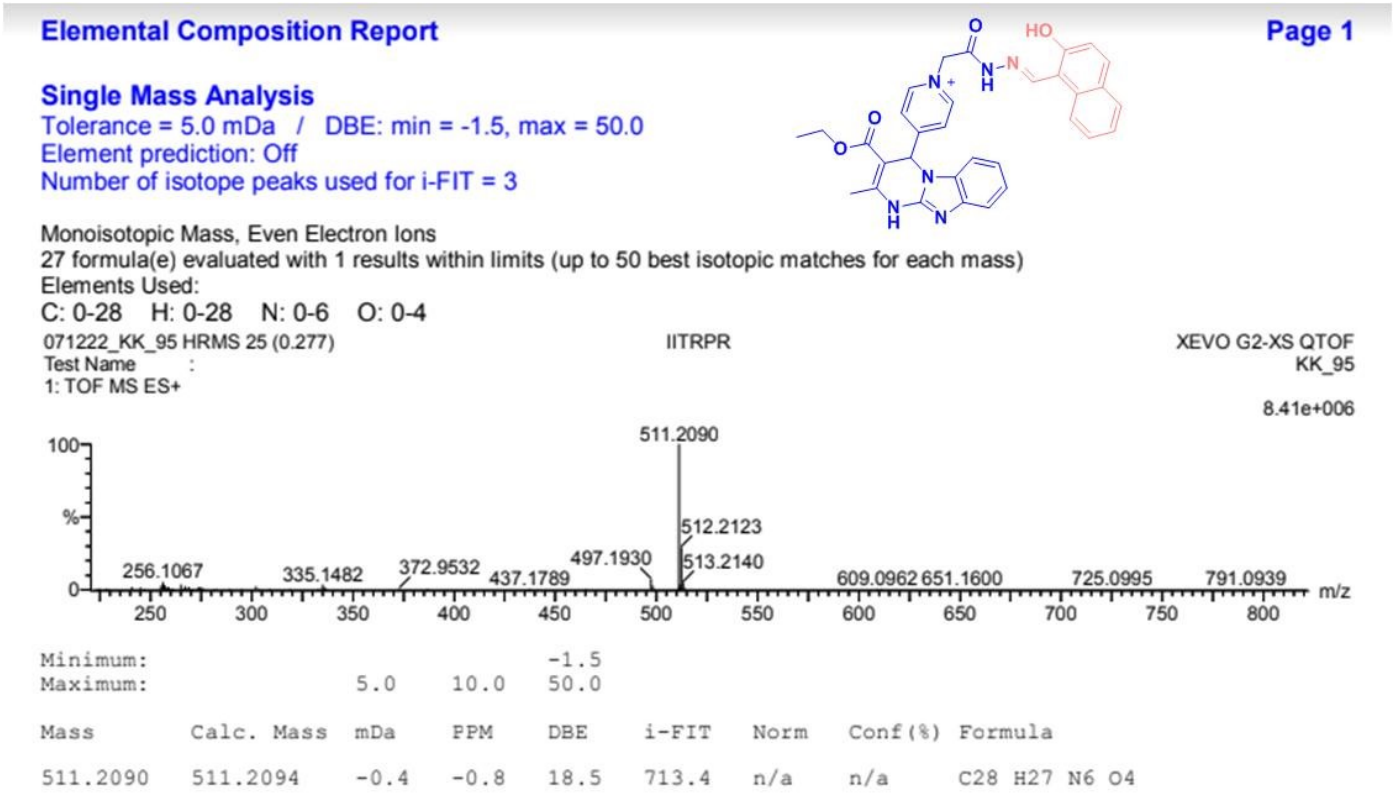

Figure S9 . HRMS of IL

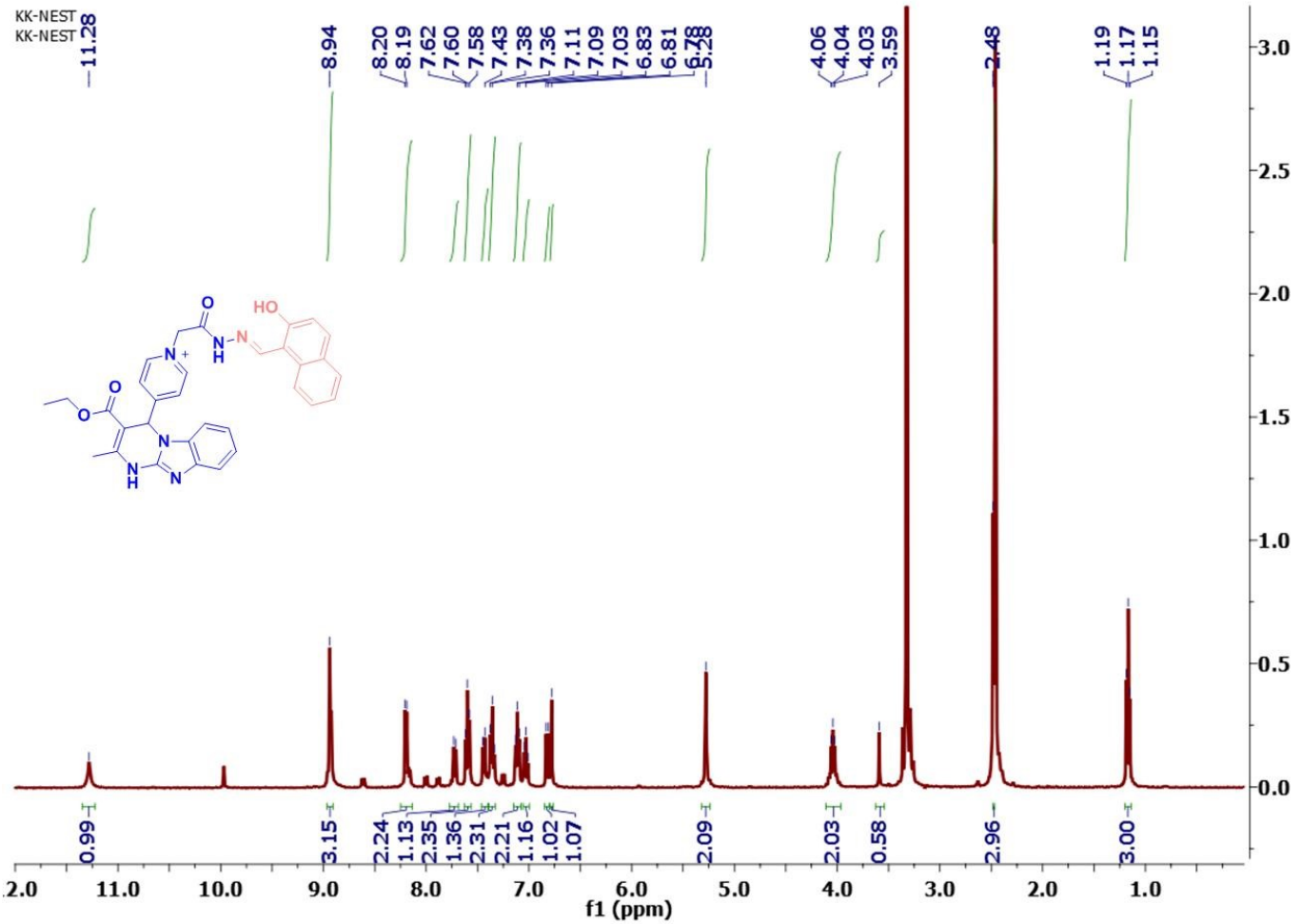

Figure S10. ^{1}H NMR spectrum of IL

^{1}H NMR (400 MHz in DMSO-d$_6$)- δ 1.17 (s, 3H), 3.59 (s, 1H, -NH), 4.06-4.03 (m, 2H), 5.28 (s, 1H), 6.83-6.81 (d, 1H), 7.03 (t, 1H), 7.11 (t, 1H), 7.36 (t, 2H), 7.45-7.43 (d, 1H), 7.60 (t, 2H), 7.73-7.71 (d, 1H), 8.20-8.19 (d, 2H), 8.94 (3H, s), 11.28 (s, -OH)

Membrane	PA (wt %)	IL@MWCNTs
PA	1.0	0
PA/IL@MWCNTs$_{2.5}$	1.0	2.5
PA/IL@MWCNTs$_5$	1.0	5
PA/IL@MWCNTs$_{7.5}$	1.0	7.5

Figure S11. Composite fabricated membranes

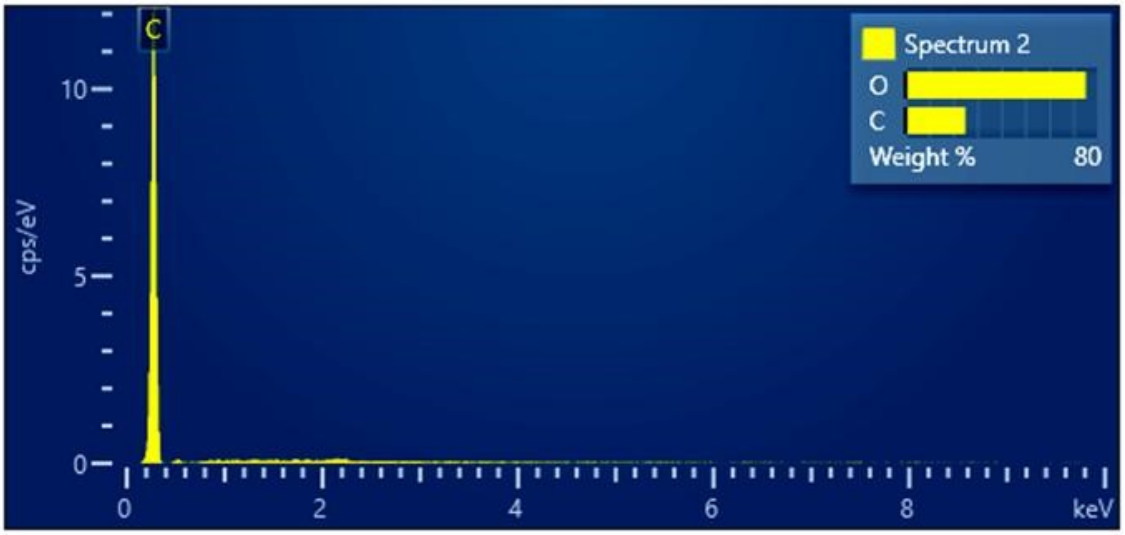

Figure S12: EDAX spectrum of bare **MWCNT**

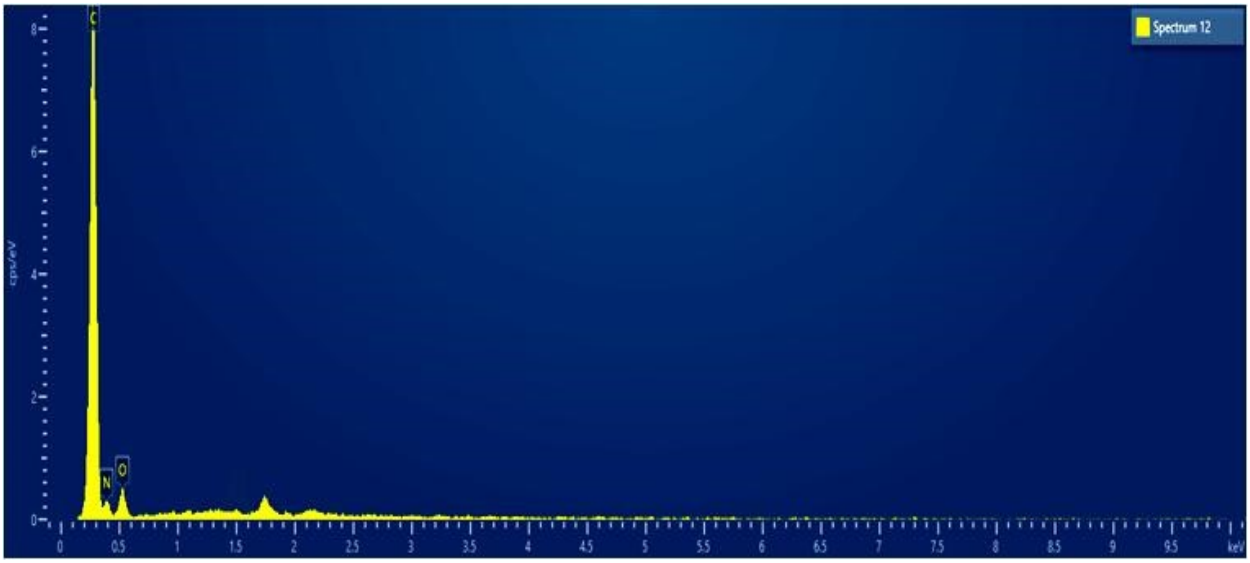

Figure S13: EDAX spectrum of **IL@MWCNTs**

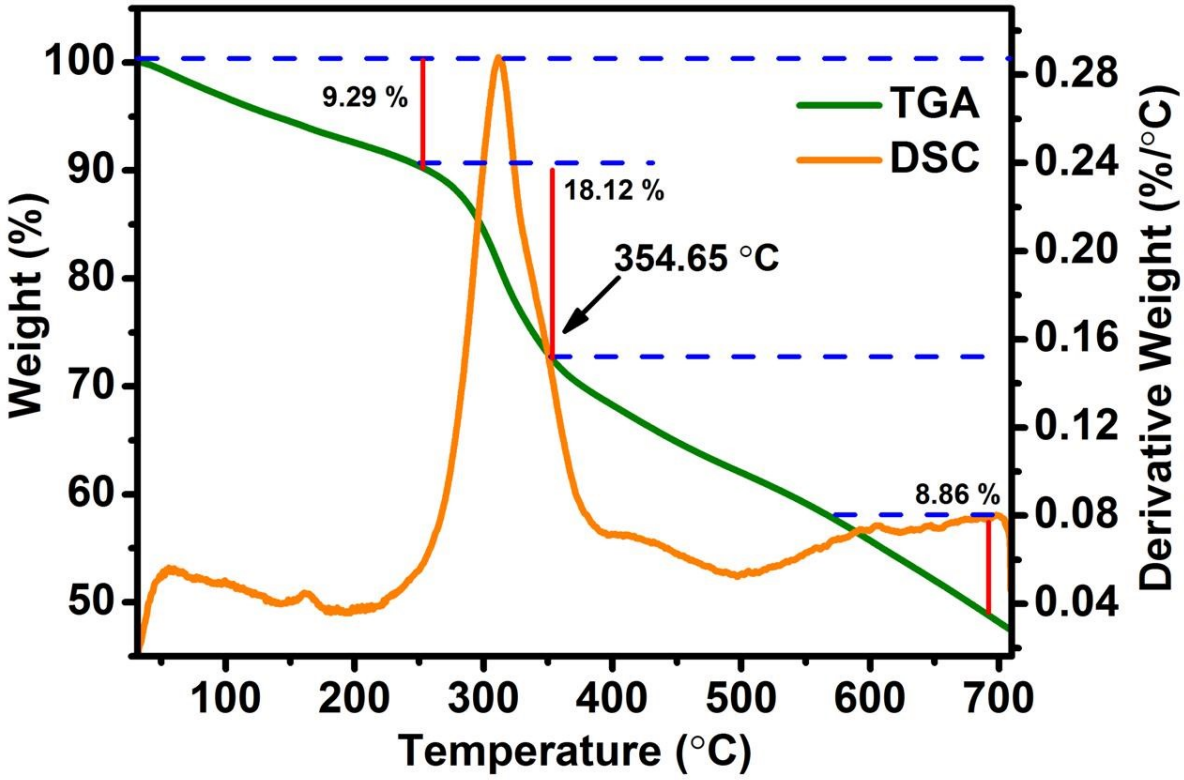

Figure S14. TGA-DSC analysis of **MWCNTs**

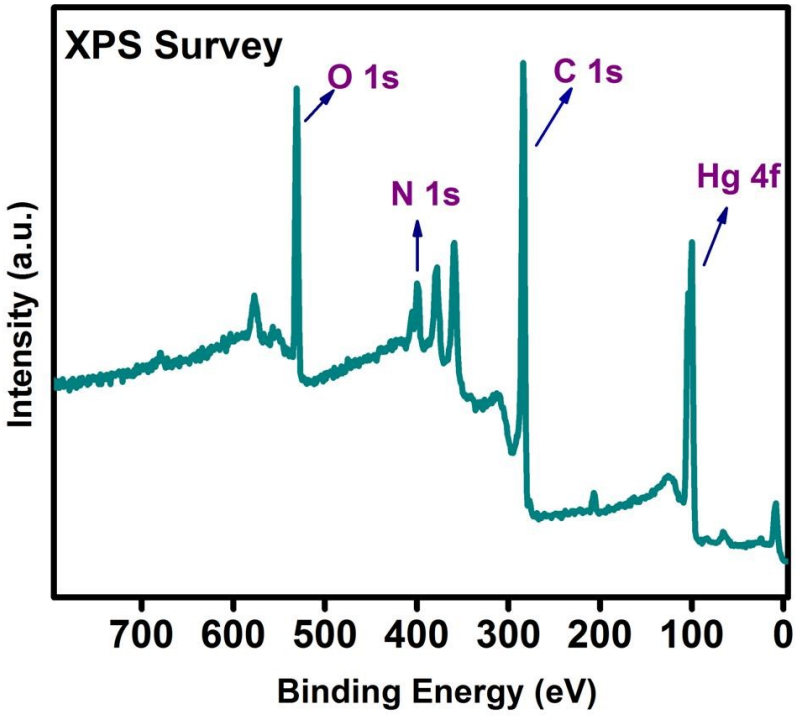

Figure S15. XPS spectrum of full region

Element	Atomic %
C 1s	70.51
N 1s	9.75
O 1s	16.62
Hg 4f	3.12

Figure S16. Peak table showing the atomic % of elements present in the **Hg/IL@MWCNTs** composite

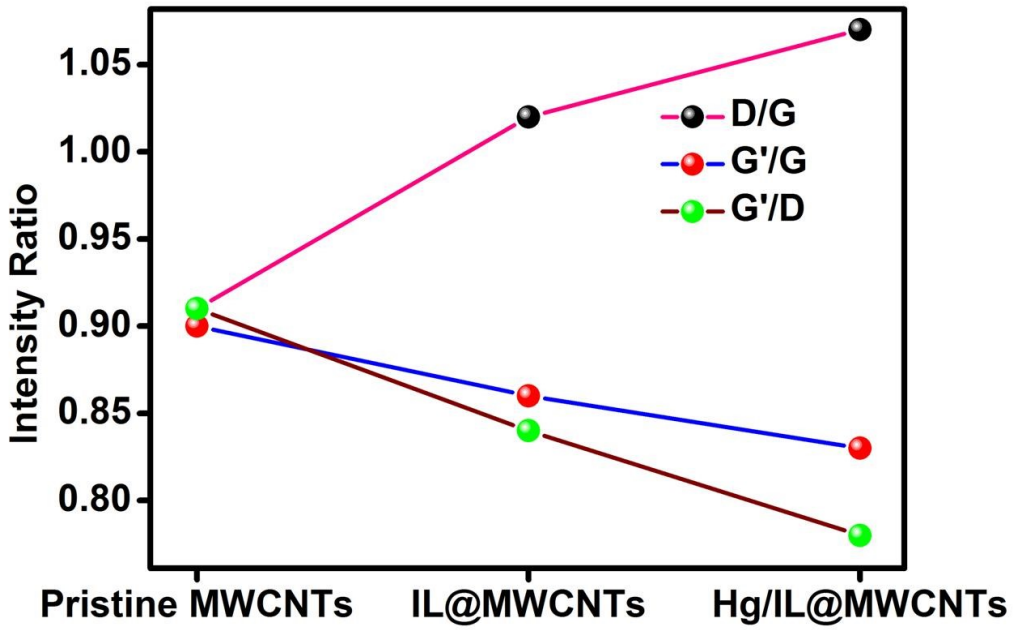

Figure S17. Relative intensity ratios of D/G, G'/G, and G'/D peaks of pristine **MWCNTs**, **IL@MWCNTs** and **Hg/IL@MWCNTs**.

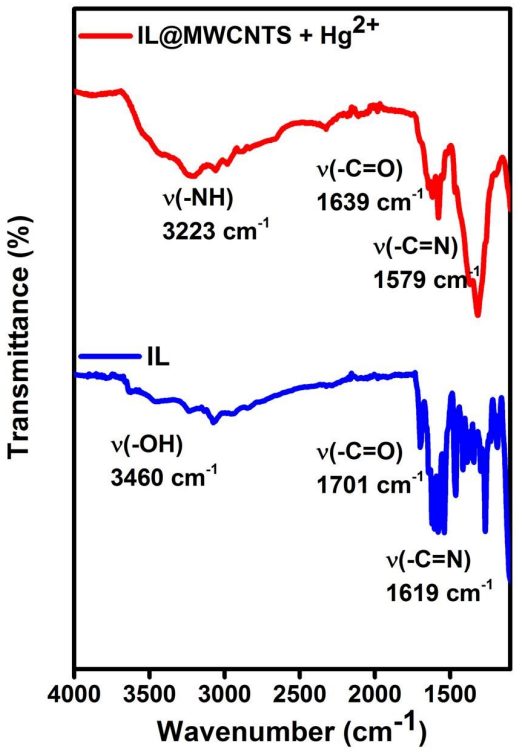

Figure S18. FTIR spectra of **IL@MWCNTs** and **IL@MWCNTs+Hg^{2+}**.

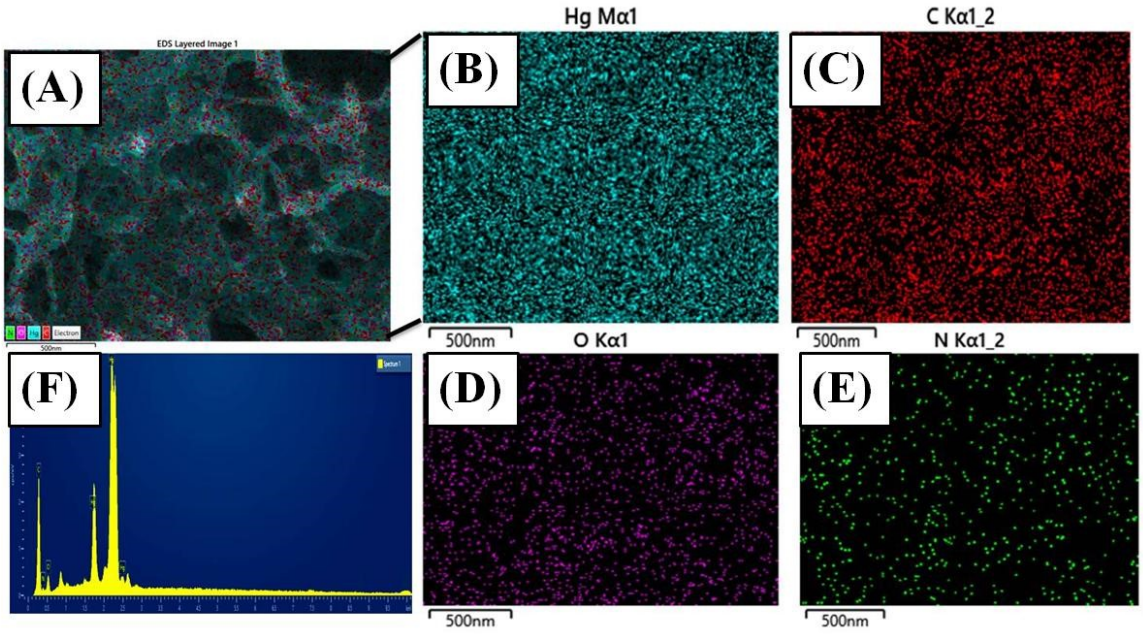

Figure S19. (A), (B), (C), (D) and (E) Bright field FE-SEM images of **Hg/IL@MWCNTs**, Elemental mapping of **Hg/IL@MWCNTs** and (F) EDAX of **Hg/IL@MWCNTs**.

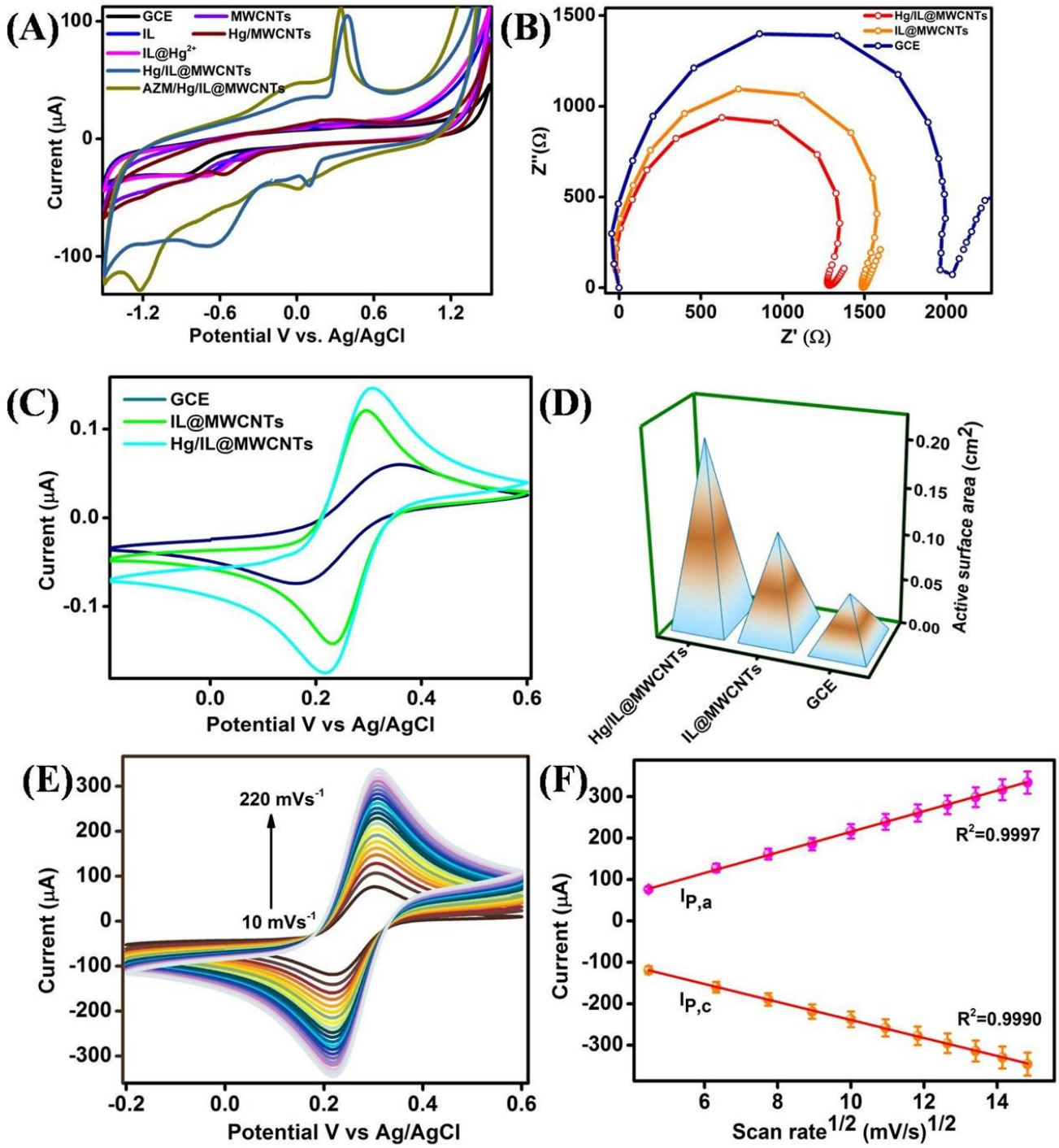

Figure S20. (A) Comparative cyclic voltammetry graphs of **bare GCE, MWCNTs@GCE, IL/GCE**, **IL@MWCNTs/GCE** and **Hg/IL@MWCNTs/GCE**, (B) EIS plot and cyclic voltammetry profiles of **bare GCE**, **IL@MWCNTs/GCE** and **Hg/IL@MWCNTs/GCE** at frequency 50 to 3×10^6 Hz, (C) Cyclic voltammetry graphs of **bare GCE**, **IL@MWCNTs/GCE** and **Hg/IL@MWCNTs/GCE** in mixture of 0.1 M KCl consisting $K_3[Fe(CN)_6]$ and $K_4[Fe(CN)_6]$, (D) Comparative profiles of active surface area with differently modified electrodes, (E) Cyclic voltammetry response of **Hg/IL@MWCNTs/GCE** with varying scan rates from 20 to 220 mV/s in a mixture 0.1 M KCl consisting of $K_3[Fe(CN)_6]$ and $K_4[Fe(CN)_6]$ solution and (F) Linear regression plot showing relationship between cathodic and anodic peak currents vs square root of scan rate.

Adsorption capacity of Hg^{2+} ions onto IL@MWCNTs

Many current Hg^{2+} sensing probes can only detect the heavy-metal ions, but cannot extract them from solution. In the present work, we endowed **IL@MWCNTs** with adsorptive and separable properties to remove the mercury ions from aqueous solution. To determine the adsorption capacities of the functionalized materials, the **IL@MWCNTs** (5 mg) samples were added to an aqueous solution containing 5, 10, 25, 40, 50, 100, 150 and 200 ppm different concentrations of Hg^{2+}. Then, the solution was stirred for 12 h at a fixed temperature (25 °C). After filtration, the final Hg^{2+} concentrations remaining in aqueous solution were determined with AAS (atomic absorption spectrometry).The equilibrium metal ions adsorption capacity was calculated for each Hg^{2+} sample using the following expression.

$$q_e = (C_o - C_e) \times V/m$$

where q_e is the adsorbent adsorption capacity (mg g^{-1}), C_0 and C_e are the initial and equilibrium concentration of Hg^{2+} ions (mg L^{-1}), m is the mass of **IL@MWCNTs**, and V is the sample volume (L). The adsorption capacities of IL@**MWCNTs** with regard to Hg^{2+} adsorption are presented in Figure 8. In order to optimize the use of adsorbents, it is important to establish the most appropriate adsorption isotherm. The adsorption results were fitted using Freundlich adsorption isotherm model supporting multilayer adsorption mechanism (**Figure 8B**). The Freundlich adsorption isotherm is expressed as follows:

$$\log Q_e = \log K_f + 1/n \log C_e \quad \text{..... (1)}$$

where q_e represents equilibrium adsorption capacity of membrane, C_e is equilibrium concentration after adsorption, k_F is the Frendulich isotherm constant and n is the heterogeneity factor, respectively. The maximum adsorption capacity for Hg^{2+} is 152.7 mg g^{-1}.

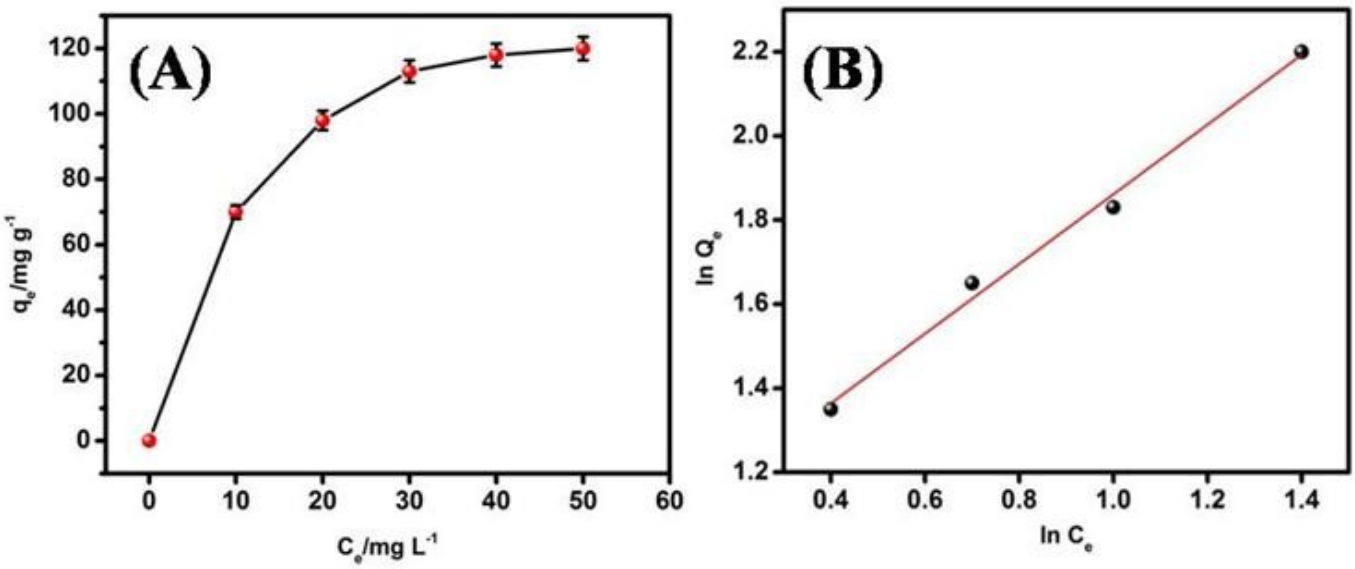

Figure S21. (A) Adsorption capacities of IL@MWCNTs with regard to Hg^{2+} adsorption and (B) Frendulich adsorption isotherm plots for Hg^{2+} adsorption onto IL@MWCNTs**.**

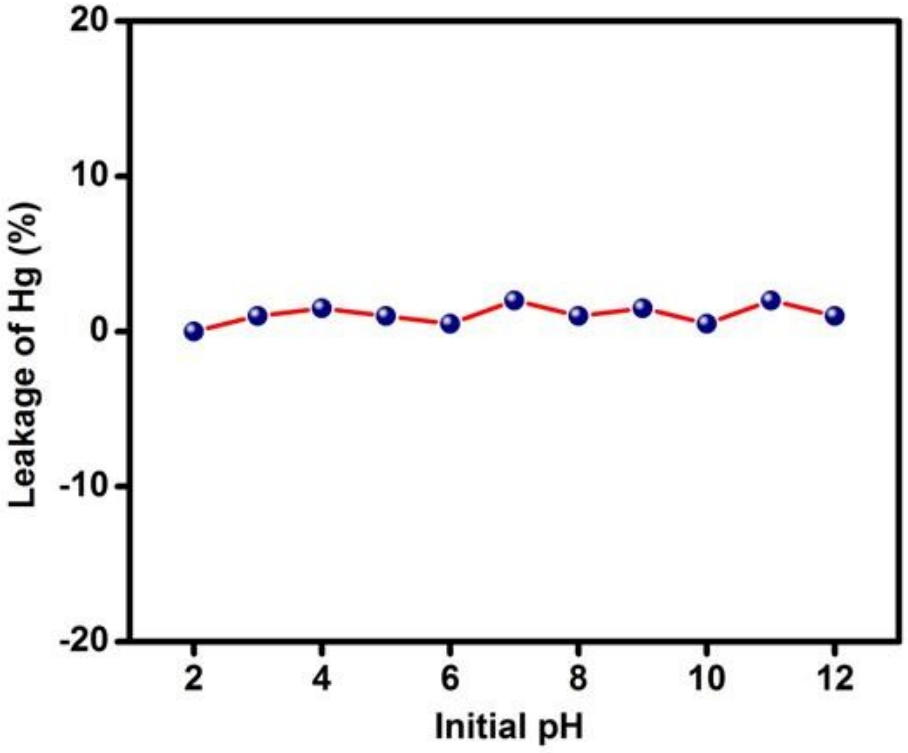

Figure S22. Leaching study of IL@MWCNTs for Hg^{2+} ion

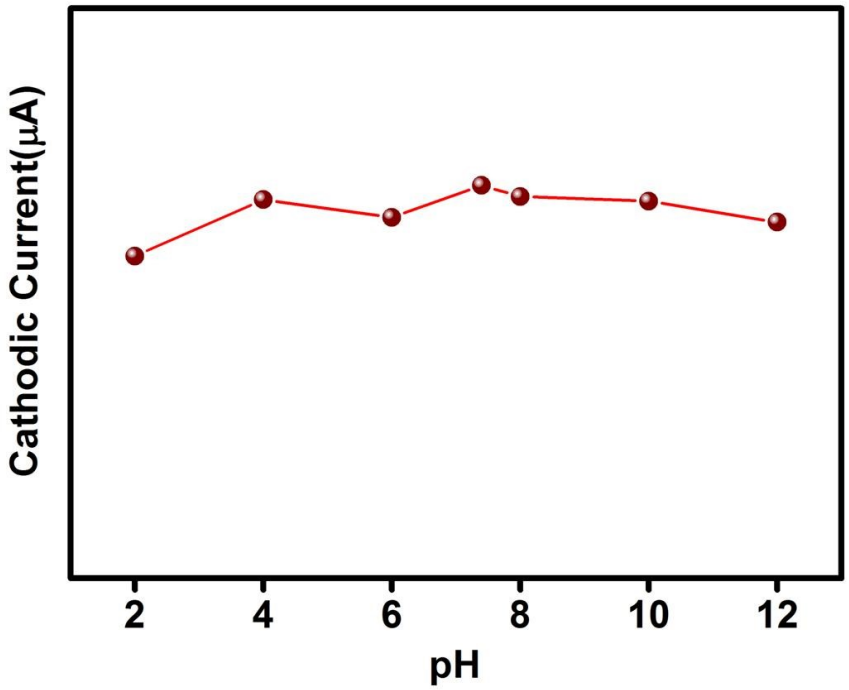

Figure S23. Effect of pH on cathodic current after addition of AZM

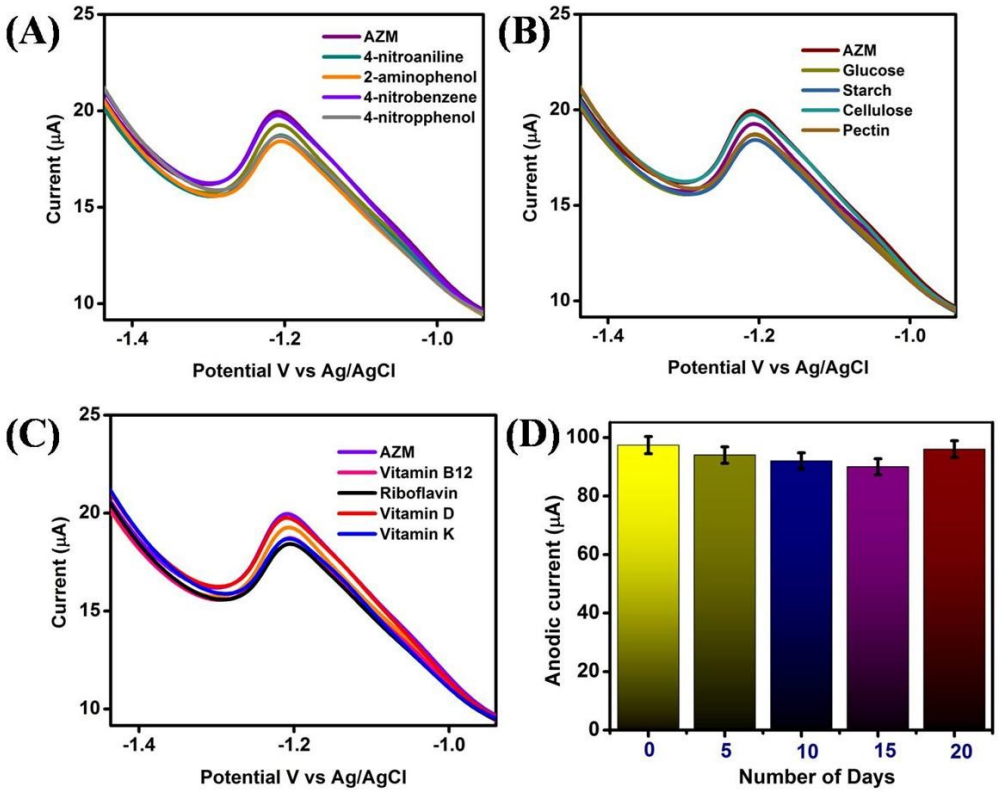

Figure S24: DPV response of Hg/IL@MWCNTs (A) nitroaromatics; (B) polysaccharides; (C) Vitamins and (D) Bar graph showing the stability of response of Hg/IL@MWCNTs for AZM detection with number of days.

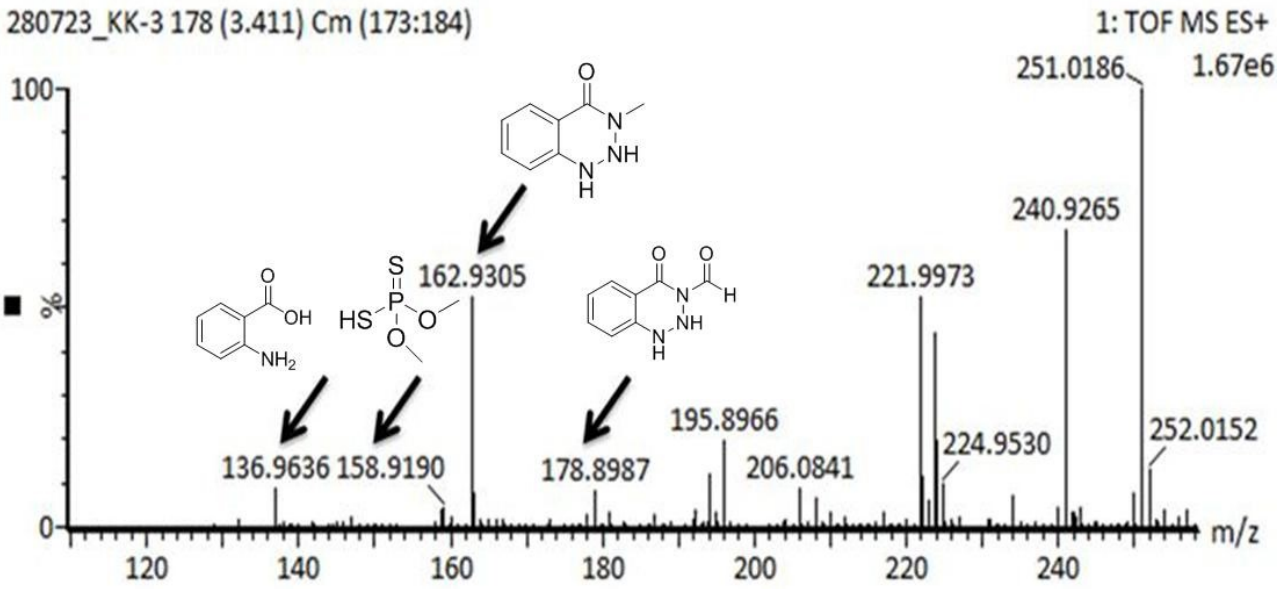

Figure S25. Mass spectra of degraded AZM products

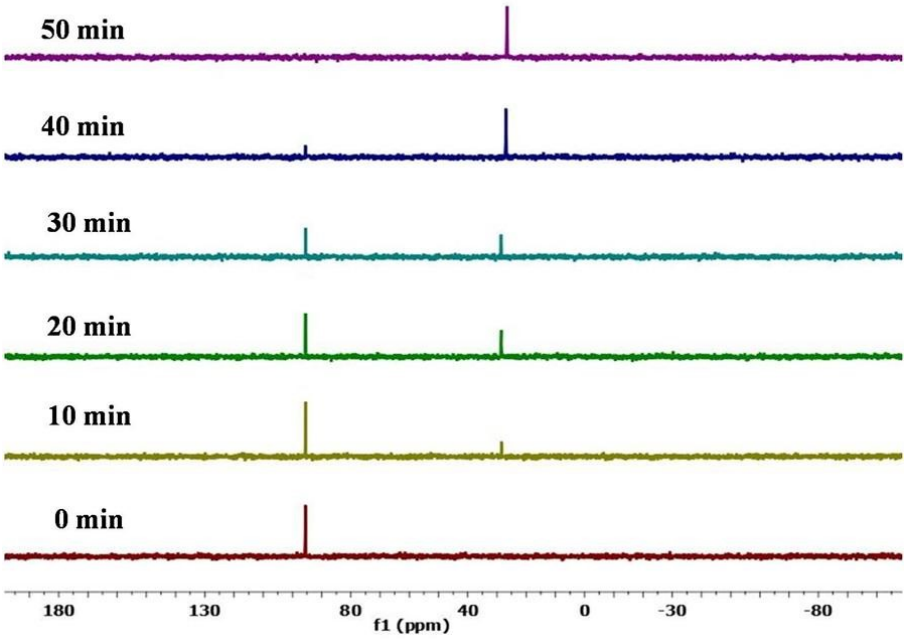

Figure S26. ^{31}P NMR spectrum obtained for AZM in presence of Hg/IL@MWCNTs catalyst in DMSO-d_6: D_2O (35:65 v/v).

Table S1

Sample	Conc. of spiked samples [µM]	Found conc. in samples [µM]	Recovery [%]	RSD[a]
Tap Water	10	9.63	96.3	0.417
	20	19.96	99.8	0.247
	30	29.86	99.5	0.103
Agriculture run-off	10	10.54	105.4	1.150
	20	20.11	100.5	1.629
	30	30.22	100.7	0.527
River Water	10	9.92	99.2	0.364
	20	19.32	96.6	1.247
	30	29.19	97.3	0.721
[a] Measurements of three experiments (n = 3)				

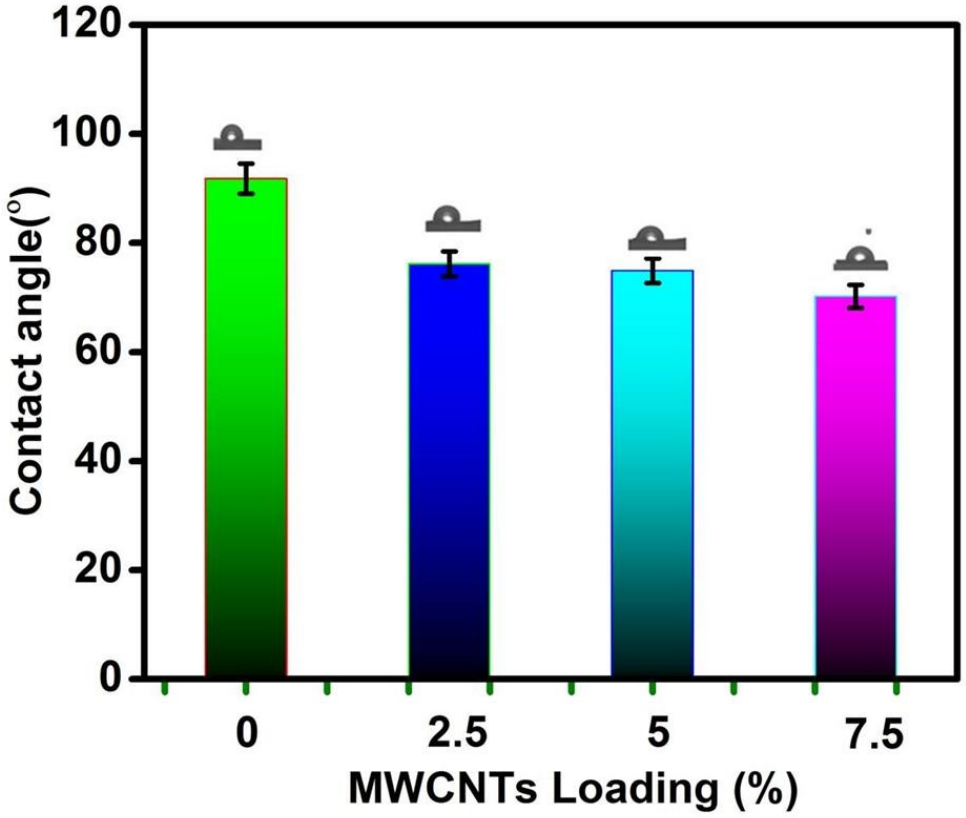

Figure S27: Contact angle measurement

Table S2

Sample	S_{BET} (m^2g^{-1})	V_{total}
PA	6.98	0.29
PA/IL@MWCNTs-2.5	61.31	0.27
PA/IL@MWCNTs-5	74.18	0.23
PA/IL@MWCNTs-7.5	87.68	0.19

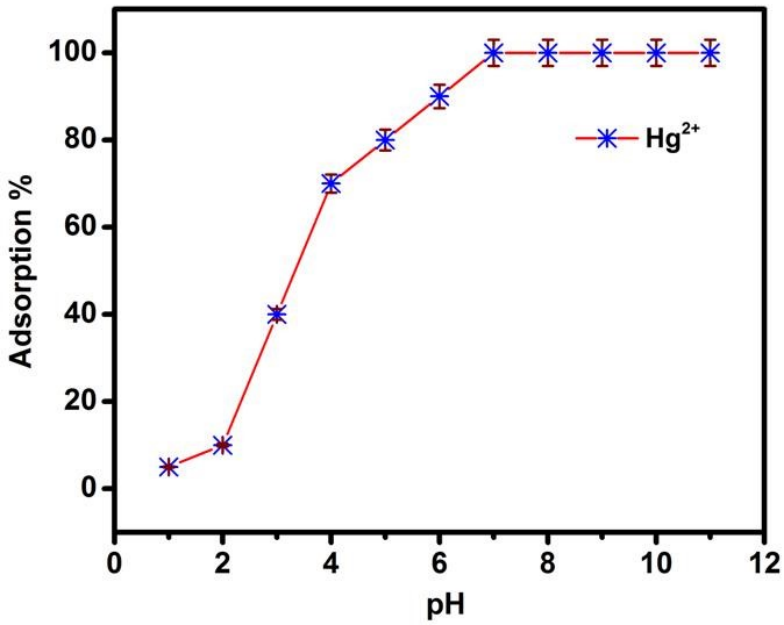

Figure S28. Influence of pH on adsorption kinectics of Hg^{2+} ion

Table S3

Volume of AZM (ml) passed through membrane (PA/IL@MWCNTS/Hg^{2+}) (Adsorbed Hg^{2+} = 19 mg Membrane = 3×3 cm^2)	**Degradation (%)**
5 ml	99.50
10 ml	97.80
15 ml	96.50
20 ml	93.50
25 ml	90.60
30 ml	89.70

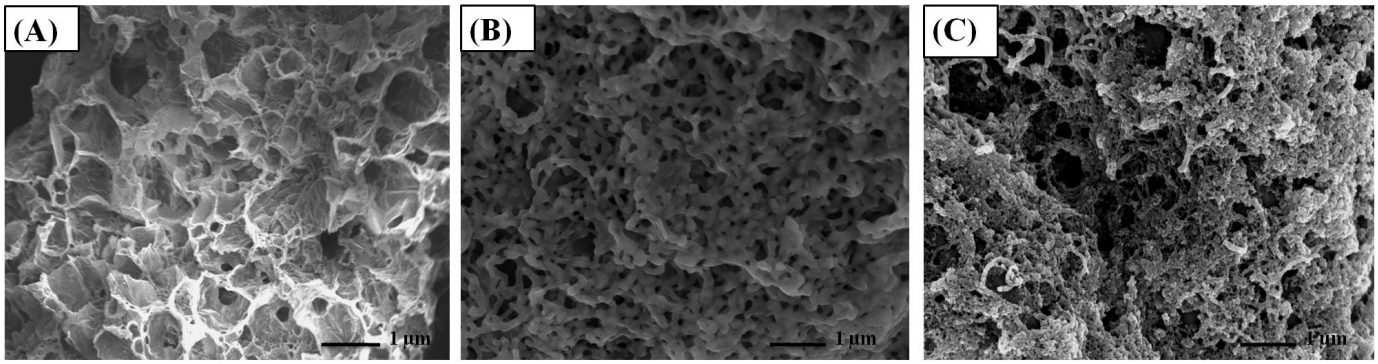

Figure S29. FE-SEM image of (A) pristine membrane, (B) PA/IL@MWCNTs membrane and (C) after filteration of Hg^{2+} and AZM.

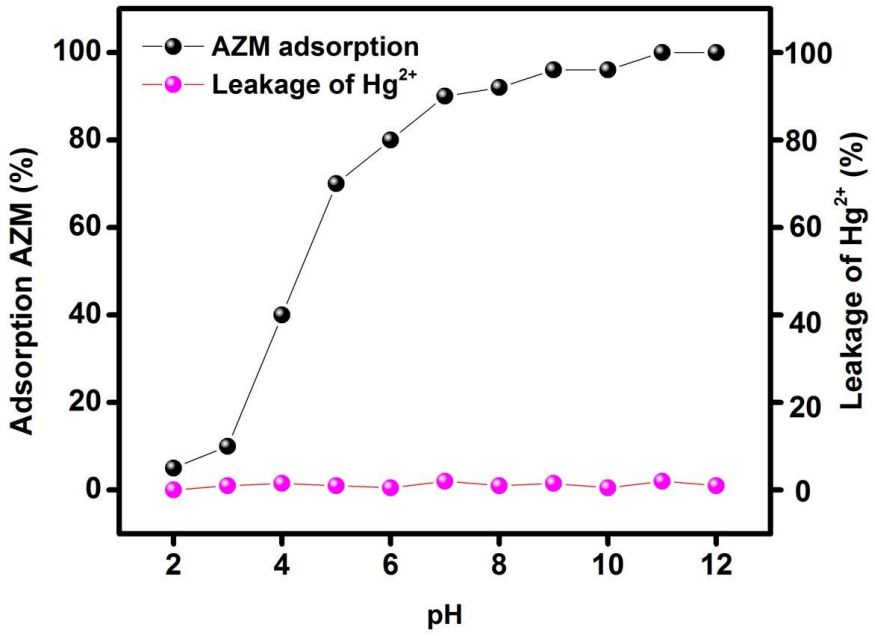

Figure S30. Influence of pH on AZM adsorption

Table S4

S.No.	Method/Probe	Quantification and Degradation	Linear range	LOD and degradation %age	Type of Real sample	References
1.	Electrochemical (Cyclic voltammetry)/ N/Cu-HPC/GCE	Quantification	0.5 μM to 60 μ M	0.026 mM	Rice	**1**
2.	GC-MS/MS and LC-MS/MS	Multiresidue analysis	-	10 ng/g	Avocado Extract	**2**
3.	Enhanced chemilumniscence enzyme linked immunosorbent	Quantification	-	9.04 mgL^{-1}	Cucumber, Cabbage	**3**
4.	Solar light photo transformation and HPLC	Detection and degradation	-	-	Clay and goethite	**4**
5.	SERS/ Graphene-AuNRs	Quantification		5 ppm	-	5
6.	Lumniscence/ MOF	Quantification	-	-	Apple and Tomato Juice	6
7.	Fluorescent chemosensor	Quantification	1 – 100 μM	5.16 μM	RO water, Tap Water and Orange Juice	**7**
8.	HPLC-photodiode array/ Fabric phase sorptive extraction	Quantification	5-700 μgL^{-1}	9.6 μg L^{-1}	Fruit juice, carrot juice and wastewater	**8**
9.	Stripping Voltammetry	Quantification	-	65.87 μg kg^{-1}	Honey	**9**
10.	**Electrochemical/ IL@MWCNTs**	**Quantification, degradation and removal**	**0.20 - 180 μM**	**1.10 μM**	**River water, agricultural run-off and**	**Present Work**

					tap water	

References

1. Q. Wang, H. Zhangsun, Y. Zhao, Y. Zhuang, Z. Xu, T. Bu, R. Li and L. Wang, Macro-meso-microporous carbon composite derived from hydrophilic metal-organic framework as high performance electrochemical sensor neonicotinoid determination, J. Hazard. Mater., 2021, 411, 125122.

2. N. Chamkasem, L.W. Ollis, T. Harmon, S. Lee, G. Mercer, Analysis of 136 pesticides in avocado using a modified QuEChERS method with LC-MS/MS and GC-MS/MS. J.Agri. Food Chem., 2013, 61, 2315–2329.

3. B. Liu, Y. Ge, Y. Zhang, Y. Song, Y. Chen, S. Wang, Development of a simplified enhanced chemiluminescence enzyme linked immunosorbent assay (ECL-ELISA) for the detection of phosmet, azinphos-methyl and azinphos-ethyl residues in vegetable samples, Anal. Methods. 2013, 5, 5938–5943.

4. M. Menager, M. Sarakha, Simulated solar light photo-transformation of organophosphorus azinphos methyl at the surface of clays and goethite. Environ. Sci. Technol. 2013, 47, 765–772.

5. T. Nguyen, Z. Zhang, A. Mustapha, H. Li, M. Lin, Use of Graphene and Gold Nanorods as Substrates for the Detection of Pesticides by Surface Enhanced Raman Spectroscopy, J. Agric. Food Chem. 2014, 62, 43, 10445–10451.

6. D. Singha, P. Majee, S. Mandal, S. Mondal, P. Mahata, Detection of Pesticides in Aqueous Medium and in Fruit Extracts Using a Three-Dimensional Metal–Organic Framework: Experimental and Computational Study, Inorg. Chem. 2018, 57, 19, 12155–12165.

7. M. Bhattu, A. Wani, M. Verma, P. Bharatam, D. Kathuria, J. Gandara, A selective turn-on fluorescent chemosensor 1,1-diaminozine for azinphos-methyl, Journal of photochemistry and photobiology A: Chemistry, 2023, 437, 114476.

8. H. Ulusoy, M. Dabbagh, M. Locatelli, S. Ulusoy, A. Kabir, M. Farajzadeh, Azinphos-methyl and chlorfenvinphos pesticides determination using fabric phase sorptive extraction followed by high performance liquid chromatography-photodiode array detector, Microchemical Journal 2023, 191, 108789.

9. C. Tsiafoulis, C. Nanos, Determination of azinphos-methyl and parathion-methyl in honey by stripping voltammetry, Electrochimica Acta, 2010, 56 (1), 566-574.